EAI Endorsed Transactions
on Ubiquitous Environments
Research Article ICST.ORG

On massive MIMO and its applications to machine type communications and FBMC-based networks

João Paulo Miranda[1,*], Arman Farhang[2], Nicola Marchetti[2], Felipe A. P. de Figueiredo[1], Fabbryccio A. C. M. Cardoso[1], Fabrício Figueiredo[1]

[1]CPqD - Research and Development Center on Telecommunication, Brazil
[2]CTVR - The Telecommunications Research Centre, Trinity College Dublin, Ireland

Abstract

We identify issues and solutions in the key area of Massive Multiple Input Multiple Output (MIMO). We illustrate the role this technology will play in 5G communications through two study cases. In the first study case, we propose a Massive Multiuser (MU)-MIMO setup to tackle the mixed-service communication problem. Our results suggest that, as the array size at the base station progressively increases, the performance of sub-optimal linear filtering approaches the perfect interference-cancellation bound. Our second study case looks at the intersection of Massive MIMO and waveform design. We introduce the self-equalization property of Filter Bank Multicarrier (FBMC)-based Massive MIMO networks, and show it can reduce the number of subcarriers required by the system. It is also shown that the blind channel tracking property of FBMC can decontaminate pilots. These findings shed light into and motivate for two exciting research lines towards a better understanding of Massive MIMO systems.

Received on 21 March 2015; accepted on 23 March 2015; published on 13 July 2015

Keywords: Filter bank multicarrier, large-scale antenna systems, machine type communications.

doi:10.4108/ue.2.5.e3

1. Motivation

Ongoing societal developments have been changing the way we use communication systems. These changes are, in part, due to the big rise in on-demand data consumption over mobile and wireless networks. One issue associated with the task of accommodating such changes consists of finding solutions that can meet the diverse needs of the use cases regarded as market drivers for Fifth Generation (5G) networks. A non-exhaustive list of 5G drivers includes broadband telephony with gigabit wireless connectivity for public safety and immersive multimedia applications, such as high-resolution video, virtual reality, and gaming [1]; Tactile Internet for real-time applications posing ultra-low latency requirements [2]; and the Internet of Things (IoT) for machine-centered communications in dense networks of bursty traffic generating devices [3].

*Corresponding author. Email: jmiranda@cpqd.com.br

Applications within the IoT driver's scope, which we shall hereafter refer to as Machine Type Communications (MTC), range from infrastructure monitoring to smart cities [4, 5], and mobile health – including telemedicine, sports and fitness – to Advanced Driver Assistance Systems (ADAS) [6, 7]. Reliability in smart grid and critical infrastructure monitoring, for instance, is often achievable only via dedicated landlines [8, 9]. Telemedicine involves the diagnostic through medical records stored in the cloud, thus calling for both real-time, low-latency access and high-capacity infrastructure capable of handling data of voluminous nature, *e.g.* magnetic resonance imaging and computerized axial tomography [10, 11]. Infotainment, pre-crash sensing and mitigation, and vehicular cooperation in ADAS also need support for high-speed, low-latency car-to-car and car-to-infrastructure communications [12–14].

As the discussion above attests, 5G requirements can be quite diverse even within a single market driver. Another issue raised by the IoT is scalability, as the current premise is that hundreds to hundred thousands of low-cost MTC devices will be served by a sole Base

Station (BS) [15]. While scalability issues have been addressed using different (sometimes complementary) approaches, such as lessons learned from duty-cycled Wireless Sensor Networks [16], waveform design for asynchronous signaling in the uplink [17], and sparse signal processing strategies [18], less is understood to date about Multiple Input Multiple Output (MIMO) techniques in the context of MTC networks.

A popular view is that the required increase in data rate will be achieved through *combined gains* [19] in extreme network densification (to improve area spectral efficiency), increased bandwidth (by exploiting mmWaves and by making better use of unlicensed spectrum), and increased spectral efficiency (through advances in MIMO techniques). A consequence of the powerful signal processing enabled by a large array sizes is that most of the scheduling and physical layer control issues in general are automatically resolved in Massive MIMO systems – which of course is not the case for systems with just a moderate number of antennas. In recent past, Massive MIMO has gained significant momentum as potential candidate to increase capacity in multi-user networks. In the limit, as the number M of antennas at the BS tends to infinity, the system processing gain tends to infinity. As a result, the effects of noise and multi-user interference are removed [20].

In this quest for bandwidth, other challenges that need be addressed in the context of 5G are fragmented spectrum and spectrum agility. It is unlikely that all these challenges can be satisfied using Orthogonal Frequency Division Multiplexing (OFDM), and new waveforms are required. Some researchers have also started to question the working assumption of strict synchronism and orthogonality in cellular networks, as a way to relax strict time-domain requirements in case of sporadic traffic generating devices (*e.g.* MTC devices) or applications requiring ultra-low latency, such as the Tactile Internet.

Waveform design is quite a hot topic at the moment, as it sheds light into how candidate waveforms perform in cellular environments, and discusses how they fare regarding specific aspects of 5G systems. In [21], for instance, OFDM is compared to Filter Bank Multi-Carrier (FBMC), Time Frequency-packed Signaling (TFS), and Single-Carrier Modulation (SCM): OFDM is preferred in terms of ease of hardware implementation; SCM is the best candidate to reduce latency and peak-to-average power ratio (PAPR); FBMC is most robust against synchronisation errors; all waveforms but TFS can be used in mm-Wave bands, and all can be adopted in a Massive MIMO setup, *i.e.* systems using arrays with at least an order of magnitude more antennas than conventional systems [22].

In general, it appears that any modulation technique, either single- or multi-carrier, can be used in combination with large antenna arrays. According to [21], it is reasonable to foresee that a similar behavior with respect to the vanishing of inter-user and Inter-symbol Interference (ISI) can be observed for any modulation format when the number of receiving antennas M is sufficiently high. However, since not all waveforms have equal advantages, the benefits of large antenna arrays can make a certain Massive MIMO-specific waveform combination more attractive than others. FBMC offers lower out-of-band (OOB) emissions, and allows less expensive and more flexible carrier aggregation than OFDM, but traditionally had the problem of non easy applicability of MIMO to it [23]. By scaling up the number of antennas, the combination of Massive MIMO and FBMC can benefit from the former's gains while still retaining the good properties of the latter [24].

In [25] it is pointed out that, because of the law of large numbers, the channel hardens so each subcarrier in a Massive MIMO system will substantially have the same channel gain. Such property is also reported in the context of FBMC in [24], where the authors name it *self-equalization*, and can lead to a reduction in the number of subcarriers required by the system. Another advantage of Massive MIMO systems is that, thanks to their many spatial degrees of freedom, the same frequency band can be reused for many users. This plus the channel hardening render frequency-domain scheduling no longer needed, making most of the physical layer control signaling redundant.

The remainder of the paper is as follows. Section II provides a brief yet comprehensive overview of Massive MIMO, its challenges, and solutions available at the time of this writing. Section III surveys the subject waveform design with focus on determining the suitability of candidate modulation formats from the perspective of several 5G-specific aspects including, of course, support for large antenna arrays. Section IV presents a study case, where the feasibility of Massive MIMO for MTC networks is investigated as means to address the uplink mixed-service communication problem. The insights gathered thus far are then exploited in a second study case in Section V, where some recent results of the authors on the combination of Massive MIMO and FBMC are discussed. Section VI wraps up the paper with concluding remarks.

2. Large-scale Multiple Antenna Systems

This section discusses issues regarded as most challenging in the Massive MIMO literature. Table 1 lists such issues and their available solutions, each presented alongside with its side effects, *i.e.* new issues brought about by their adoption.

2.1. Impairments due to Low-cost Hardware

Large-scale multiple antenna arrays will likely be built using low-cost components to ease the introduction

Table 1. Summary of Challenges & Solutions in Large-scale Multiple Antenna Systems for 5G.

Research Area	Issue	Candidate Solutions		Shortcomings and "Side Effects"	Refs
Hardware	Phase noise	Smart PHY transceiver algorithms		Efficacy yet to be demonstrated	[25]
	Power consumption	Parallel, dedicated baseband processing		Open research question	
	Proof-of-Concept	Experiments, testbeds & prototypes		Only basic capabilities demonstrated	[26]
Antenna Aspects	Antenna coupling	Multiport impedance matching RF circuits		• Diminishes bandwidth • Introduces ohmic losses • Not fully understood for large M	[27–31]
	Front-back ambiguity	Dense multidimensional implementations		• Increases coupling effects • Limited to indoor environments • 3D arrays have restricted usefulness	[27, 32]
Propagation	Channel modeling	• Realistic empirical models • Sophisticated analytical models		Currently under development	[33, 34]
	Cluster resolution	No solution known to date		Open research question	[22]
Transceiver Design	CSI acquisition	BS sends pilots to terminals via FDD		Limited by the channel coherence time	[20, 35]
		Terminals send pilots to BS via TDD		Channel reciprocity calibration	[36–39]
				Pilot contamination problem	[40–43]
	Precoding	Linear precoding methods	• ZF • MMSE	• Computationally heavy for large M • Higher average transmit power	[22, 44]
			• MF	• Has an error floor as M increases • Higher M required for a given SINR	[22]
			• BD	Cost-effective strategies are needed	[45]
		Nonlinear precoding methods	• DPC	Extremely costly for practical deployment	[46]
			• THP • VP	Increased complexity is hard to justify	[47] [48]
	Detection	Linear filtering	• MRC	• Does not treat interference suppression	[20]
			• ZF	• Does not treat noise enhancement	[49]
			• MMSE	• More complex than MRC	[22, 72]
		Iterative linear filtering	• MMSE-SIC • BI-GDFE	Computationally heavy for large M	[50]
		Random step search methods	• TS • LAS	More complex than MMSE-SIC	[51] [52]
		Tree-based algorithms	• SD	Complexity grows exponentially in M	[53]
			• FCSD	• 1,000x more complex than TS • Best suitable for the $M \approx K$ case	[54]

and leverage the penetration of the Massive MIMO technology into the market. This calls for solutions capable of circumventing hardware imperfections that manifest themselves as I/Q imbalance or phase noise. The latter issue is of particular concern because low-cost power amplifiers often have relaxed linearity requirements, which in turn translate into the need for reduced PAPR on a per antenna element basis [25].

Savings in radiated power result from using excess antennas to simultaneously send independent data to different users, but the total power consumption should also be taken into account. In this context, an interesting research path is hardware architectures for baseband signal processing [25]. Another path of interest is experimentation, as testbeds currently available only demonstrate basic capabilities, and do not take constrained BS real estates into consideration [26]. Experimentation can also be rewarding in that experimental findings can be fed back into theory, thus rendering the development of testbeds, prototypes, and proof-of-concept experiments of utmost importance to a better understanding about the technology.

2.2. Mutual Coupling and Front-back Ambiguity

One assumption often made when modeling antenna arrays is that the separation among antenna elements is large enough to keep mutual coupling at negligible levels. This is not entirely realistic, especially in the case of a large number of antenna elements deployed as an array of constrained size and aperture. Under such practical conditions, mutual coupling is known to substantially impact the achievable system capacity [27]. Multiport impedance matching RF circuits can cancel out such coupling effects [28], but they diminish output port bandwidth [29] and increase ohmic losses [30, Chapter 10].

Two- or three-dimensional arrays have been reported able to avoid front-back ambiguity. A side effect of

dense implementations is that the larger the number of adjacent elements, the larger the increase of coupling effects [22]. Another fundamental shortcoming specific to 3-D settings is the incapability of extracting additional information from the elements inside the array, *i.e.* only elements on the array surface contribute to the information capacity [32]. The optimal densities above which performance deteriorates no matter how large is the number of elements are studied in [31] for indoor Massive MIMO BSs.

2.3. RF Propagation and Channel Modeling

Realistic performance assessments call for appropriate channel characterization and modeling. The Massive MIMO channel behavior, including its correlation properties and the influence of different antenna arrangements, cannot be captured otherwise. The interest raised by this issue has been (and still is) experiencing a fast-paced growth, and the community has already managed to contribute towards a better understanding on the matter. In [33], channel measurements are carried out to identify and statistically model the propagation characteristics of interest. These are then fed back into an existing channel model, extending its applicability to large-scale antenna arrays.

Performance assessments should ideally be conducted using a standardized or widely accepted channel model. At the time of writing, no such a model seems to exist for Massive MIMO. See, *e.g.* [34], for a discussion on modeling methods, channel categories, and their underlying properties.

2.4. Acquisition of Channel State Information

In conventional systems, the BS cannot harness beamforming gains until it has established a communication link with the terminals. Firstly, the BS broadcasts pilots based on which the terminals estimate their corresponding channel responses. These terminal estimates are then quantized and fed back to the BS. Such Frequency-division Duplexing (FDD) finds limited application in Massive MIMO systems in that the amount of time-frequency resources needed for pilot transmission in the downlink (DL) scales as the number of antennas, and so does the number of channel responses that must be estimated on the part of each terminal. In large arrays, pilot transmission time may well exceed the coherence time of the channel [20, 35].

An alternative for Massive MIMO systems is to let the terminals send pilots to the BS via Time-division Duplexing (TDD). The TDD approach relies on channel reciprocity, where uplink (UL) channels serve as estimate of DL channels. This leads to training requirements independent of M [36], and eliminates the need for Channel State Information (CSI) feedback. TDD's drawbacks are reciprocity calibration and pilot contamination: the former is a need raised by different transfer characteristics of DL/UL; the latter arises in multi-user scenarios where the use of non-orthogonal pilot sequences causes the intended user's channel estimate to get contaminated by a linear combination of other users' channels sharing that same pilot. Reciprocity calibration and pilot decontamination are studied in [37–39] and [40–43], but optimal solutions are unknown to date.

2.5. Precoding

Multi-user interference can be mitigated at the transmit side by modifying standard single-stream beamforming techniques to support multiple streams. Precoding based on Zero-Forcing (ZF) or Minimum Mean Square Error (MMSE) is simple for a antenna numbers up to moderate. However, reliance on channel inversions may take its complexity and power burdens to a point hard to accommodate within very large arrays [22, 44]. Matched Filtering (MF), which comprises Maximum Ratio Transmission (MRT) in the DL and Maximum Ratio Combining (MRC) in the UL, is known to be the simplest method [20].

Nonlinear precoding methods, such as Dirty Paper Coding (DPC) [46], Tomlinson-Harashima Precoding (THP) [47], and Vector Perturbation (VP) [48], also have appealing features (DPC is theoretically optimal) but are either too costly for practical deployment or offer gains hard to justify in view of their increased computational complexity. Recalling that the array size required to achieve a given Signal-to-Interference and Noise Ratio (SINR) with MF is at least two orders of magnitude larger than with ZF [22], further work on cost-effective solutions is needed, *e.g.* as illustrated in [45] for Block Diagonalization (BD) algorithms.

2.6. Detection

When it comes to data streams separation in conventional systems, Maximum Likelihood (ML) detection is optimum solution but its complexity grows exponentially with the number of streams (this makes it hard to implement in MTC networks where hundreds to thousands of devices are envisioned). This is the reason why parameter estimation and detection are key problems in Massive MIMO systems. Suboptimal linear filtering detectors with reduced computational complexity, such as MRC, ZF, and MMSE [49], offer lower costs (that do not depend on the modulation), but are not capable of achieving the full receive-diversity order of ML detection [44]. This performance-complexity tradeoff led to the development of several alternative detection methods, some of them are discussed in the sequel.

The first class of interest is iterative linear filtering, which encompasses MMSE with Successive Interference

Table 2. Waveforms Regarded as Most Promising for 5G with CP-OFDM used as Benchmark (TBI = remains to be investigated).

	Figure of Merit	CP-OFDM	NC-OFDM	DFT-s-OFDM	BFDM	FBMC	GFDM	UFMC
Performance	PAPR	High	High	Reduced	High	High	Reduced	High
	Spectral Efficiency	Low	Low	Low	High	High	High	High
	Overhead	High	High	Variable	Low	Low	Variable	Low
	Frequency Localization	Good	Good	Very good	Controllable	Excellent	Excellent	Excellent
	OOB Emissions	High	Reduced	Reduced	Variable	Negligible	Reduced	Reduced
	Sidelobe Attenuation	13 dB	20–50 dB	40–60 dB	13–60 dB	60 dB	35 dB	40–60 dB
	BER	Good	Good	Good	Good	Good	Average	Very good
	Throughput	Low	Low	Low	High	High	High	High
	Time Offsets	Poor	Good	Good	Good	Good	Good	Good
	Frequency Offsets	Poor	Good	Good	Good	Good	Good	Good
Feasibility	Complexity	Low	Low	Low	High	High	High	High
	Implementation	Efficient	Efficient	Efficient	TBI	Efficient	Efficient	Efficient
	Equalization	Simple	Simple	Simple	TBI	Involved	Simple	Involved
	Resource Allocation	Dynamic and fine grained	Dynamic and fine grained	Dynamic and fine grained	Possible	Configurable	Configurable and adaptable	Configurable
Support for	Conventional MIMO	Yes	Yes	Yes	TBI	No	Yes	Yes
	High-order Modulation	Yes	Yes	Yes	TBI	TBI	Yes	TBI
	Short-burst Traffic	No	Yes	Yes	Yes	No	Yes	Yes
	Fragmented Spectrum	No	Yes	Yes	Yes	Yes	Yes	Yes
	Low Latency	No	No	No	No	No	Yes	No
	References	[19–21, 23]	[55]	[56, 57]	[59]	[3, 19, 23, 58]	[60, 61]	[3, 19, 64]

Cancellation (MMSE-SIC) and Block-iterative Generalized Decision Feedback Equalization (BI-GDFE) [50]. A shortcoming common to such iterative detectors is that their reliance on repeated matrix inversions may be render them computationally heavy for large array sizes. Tabu Search (TS) [51] and Likelihood Ascent Search (LAS) [52] belong to a class of matrix-inversion free detectors known as random step search detection methods. Regrettably, the performance-complexity tradeoff comes into play also here, as both TS and LAS are known to be outperformed by MMSE-SIC [22]. The last relevant class, referred to as tree-based detection algorithms, has in Fixed Complexity Sphere Decoding (FCSD) one of its most prominent methods [53, 54]. Notwithstanding the improvements of FCSD over standard sphere decoding, the method is still 1,000 times more complex than TS.

3. Waveform Design for 5G

Another topic of interest is waveform design, whereby candidate modulation formats are assessed *w.r.t.* specific aspects of 5G systems. In general, it appears that any modulation technique, either single- or multi-carrier, can be used in combination with large antenna arrays. However, since not all waveforms have equal advantages, the benefits of large antenna arrays can make a certain Massive MIMO-specific waveform combination more attractive than others.

Seeking to provide a better understanding about this interesting subject, we review in this section the state of the art about candidate waveforms for 5G. The discussion that follows will help us put together a second study case on the application of Massive MIMO for 5G wireless communication systems. Unless mentioned otherwise, the comparisons in Table 2 are based on the best possible performance of each waveform with OFDM with cyclic prefix (CP-OFDM) used as benchmark.

3.1. The Baseline OFDM and its Enhancements

Despite of the advantages that led to its near-universal adoption, CP-OFDM is not without its limitations [23]. High PAPR in Massive MIMO is a concern, as it sets up a tradeoff between the amplifier's linearity and cost. MmWave deployment may also prove hard due to the difficulty to develop efficient amplifiers [19]. Spectral efficiency [3] can be improved using shorter CP lengths, and Frequency and Quadrature Amplitude Modulation (FQAM) to boost DL throughput for cell-edge users. TFS and faster-than-Nyquist signaling have been claimed able to offer efficiency gains on the order of 25% over conventional OFDM (see, *e.g.* [19, 21] and the references therein). Other drawbacks of CP-OFDM are sensitivity to phase noise and asynchronous signaling, poor spectrum localization, large OOB emissions, and long round-trip time.

The amount of implementation experience and knowledge about the tricky aspects of OFDM available today make it possible to modify its baseline form to create new schemes capable of circumventing most of

its inherent limitations. Improved sidelobe suppression for dynamic spectrum access and fragmented spectrum use is claimed achievable using noncontiguous waveforms, such as Cancellation Carriers (CC) or Edge Windowing (EW). In [55], CC-OFDM with a single cancellation carrier is shown better than both its variant with multiple (weighted) cancellation carriers and EW-OFDM, but suppression performance degrades as the subcarrier index runs away from the gap edge.

Another option consists of manipulating OFDM to mimic SCM [19, 21] to reduce PAPR and provide robustness against frequency offsets. Discrete Fourier Transform spread OFDM (DFT-s-OFDM) enhances noise in faded channels, offers poor spectral containment, and allows neither frequency-selective scheduling nor link adaptation. These limitations are overcome by employing zero-tail DFT-s-OFDM, exploiting receiver diversity, and appying the DFT spread at the physical resource blocks level [56, 57]. Improved flexibility (dynamic overhead adaptation instead of hardcoded CP) and OOB emissions (smoother transitions between adjacent symbols) are additional advantages of zero-tail DFT-s-OFDM over CP-OFDM.

3.2. Filter Bank Multicarrier

FBMC introduced multicarrier techniques over two decades before the introduction of OFDM in wireless communications systems [23]. While OFDM relies on CP to prevent ISI and convert the channel into a flat-gain subcarriers set, FBMC exploits the fact that narrow and numerous subcarriers can be characterized by a flat gain. The length and superior frequency localization of FBMC prototype filters allow the terminal to deal with high delay spreads and compensate frequency offsets without feedback to the BS [3, 19] (at the expense of increased computational complexity, latency, and equalization requirements).

Fast-convolution based highly tunable multirate filter banks are investigated in [58]. Capable of implementing waveform processing for multiple single-carrier and/or multicarrier transmission channels with nonuniform bandwidths and subchannel spacings simultaneously, this method is a competitive option in terms of spectral containment and complexity.

3.3. "Born-to-be-5G" Waveforms

In contrast to FBMC or OFDM, which apart from enhancements like CC-OFDM and DFT-s-OFDM were not originally designed bearing 5G requirements in mind, we have recently witnessed the outbreak of waveforms crafted for MTC and the Tactile Internet. Biorthogonal Frequency Division Multiplexing (BFDM) waveforms, for instance, have been regarded suitable to support sporadic traffic and asynchronous signaling. One appealing feature of BFDM is time and spectral localization balancing through iterative interference cancellation, which in turn allows to control degradations due to time and frequency offsets [59].

Rendered attractive for nonsynchronous burst transmissions by its block-based structure, Generalized Frequency Division Multiplexing (GFDM) was originally proposed as a nonorthogonal alternative to FBMC. GFDM can be set to mimic OFDM, although its benefits are better experienced with SCM setups, *e.g.* to transmit multiple symbols per subcarrier. To the best of our knowledge, GFDM is the only 5G candidate waveform for which support for High-order Modulation (HOM) and Tactile Internet has been explicitly investigated.

The reader is referred to [60, 61] for a comprehensive analysis of characteristics, relevant features, performance, and implementation aspects of GFDM. Recently, performance under timing and carrier frequency offsets, and the design of low complexity transceivers for GFDM were considered in [62] and [63], respectively.

3.4. Universal Filtered Multicarrier

Another distinguishing aspect of OFDM and FBMC is that the former filters the whole signal band, while the latter works on a per subcarrier basis. Universal Filtered Multicarrier (UFMC) has been advanced as a more general solution because its filtering is applied on the level of multiple subcarriers, *e.g.* on a per resource block basis. As compared with OFDM, UFMC offers better spectral efficiency and robustness against time and frequency offsets [3, 19]. Some advantages of UFMC over FBMC are lower latency (due to its shorter filter lengths), reduced overhead, and improved support for MTC [3, 64] – although both may require more involved multi-tap equalizers.

4. Study Case I: The Uplink Mixed-service Communication Problem

In this study case, we investigate the feasibility of Massive Multiuser (MU)-MIMO as a means to address the so-called uplink mixed-service communication problem, where a *single* BS simultaneously delivers narrowband services to *both* MTC devices *and* Fourth Generation (4G) wideband services to User Equipment (UEs). Treating MTC devices as regular UEs turns out to be an issue, as scheduling Physical Resource Blocks (PRBs) in extremely dense networks is a nontrivial task made harder in the presence of retransmissions and intrinsic uplink synchronization procedures [65–68].

Assuming an available Physical Narrowband Shared Channel (PNSCH), devised to consume traffic generated by MTC devices, the capacity of the MTC network – and, in turn, that of the mixed-service system – can be increased by clustering MTC devices and letting clusters share the same time-frequency PRBs. The idea

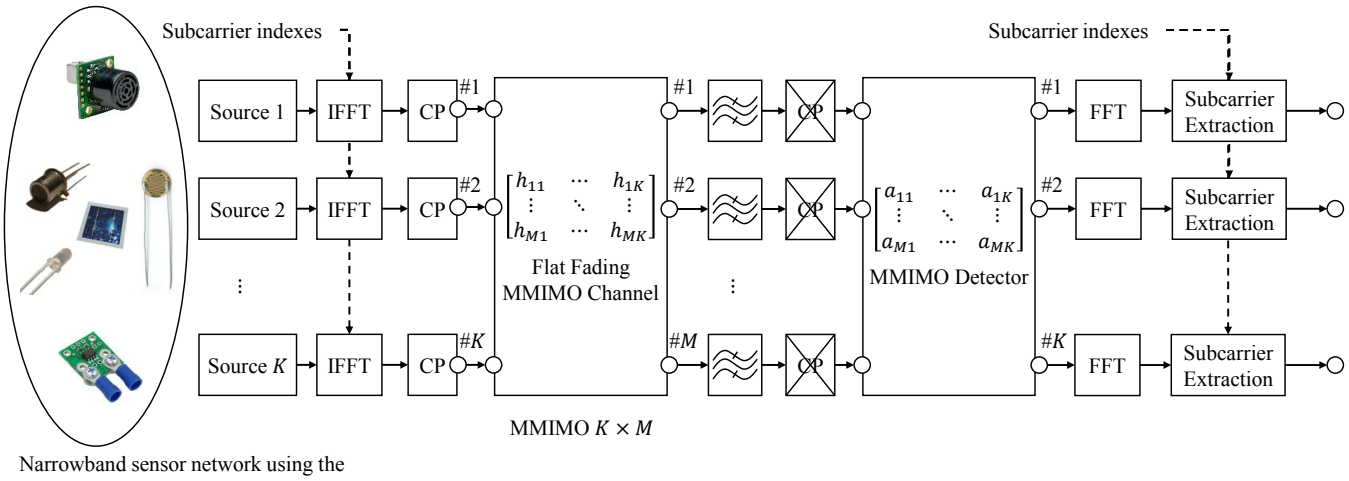

Figure 4. Block diagram of a Massive MU-MIMO uplink for mixed networks, where the BS simultaneously serves narrowband MTC devices and wideband UEs. The cluster of MTC devices seen at the transmit side share the same time-frequency PRBs, while the sole BS at the receive side is equipped with an antenna array at least one order of magnitude larger than the number of MTC devices.

behind the PNSCH is to allow the exploitation of the channel's geometric scattering characteristics to spread MTC signals in the spatial domain. The individual data streams conveyed by spatially spread MTC signals can be separated thanks to the powerful processing gain of our Massive MU-MIMO setup [20], where the antenna array size at the BS is at least one order of magnitude larger than the number of served MTC devices.

4.1. System Model

Here we describe the system depicted in Figure 1 in terms of its underlying functional blocks. We assume the transmitted signals of a cluster with K single-antenna MTC devices are detected by a Massive MU-MIMO BS equipped with M receive antennas, $M \gg K$. All the K MTC sources map data into a set of continuous PRBs in the frequency domain, with the subcarrier indexes providing the spectral position of the PNSCH at the physical layer level. The PNSCH is configured at the BS via broadcasting system information blocks, just like the physical random access channel used in current 4G systems (see, *e.g.* [69] and the references therein). This allows the number of PNSCH transmission opportunities in the uplink to be scheduled while taking into consideration discrepancies between the (likely different) capacities of MTC devices and UEs.

Each MTC device transmits a signal by taking the Inverse Fast Fourier Transform (IFFT) of the mapped data, and subsequently adding a CP. The different signal bandwidths occupied by MTC devices and UEs cause the former and the latter to respectively experience flat and frequency selective fading. The CP is thus required to ascertain compatibility in the uplink for narrowband services (MTC devices) and wideband services (regular UEs). We assume OFDM block-based transmissions, where the frequency-domain data symbols are randomly and independently drawn from a Phase Shift Keying (PSK) alphabet with normalized average energy.

Let $x_k[n]$ denote the transmitted time-domain samples of the kth MTC device, $k = 1, \ldots, K$. Assume OFDM symbols are normalized to unit variance, so $E[|x_k[n]|^2] = 1$. The power level of subcarriers not mapped with data is set to zero. In the uplink, the signals due to all K MTC devices can be collected into the vector [70]

$$\mathbf{x} = [x_1, \ldots, x_K]^T, \tag{1}$$

where $(\cdot)^T$ denotes transposition and $\mathbf{x} \in \mathbb{C}^{K\times 1}$. Hereafter, for ease of notation, we shall write simply $\mathbf{x}$ and assume that the functional dependence on the time index n is implicit.

Let $h_{m,k}$ denote the channel coefficient from the k-th MTC device to the m-th antenna of the BS

$$h_{m,k} = g_{m,k}\sqrt{d_k}, \tag{2}$$

where $g_{m,k}$ is a complex small-scale fading coefficient, and d_k is an amplitude coefficient that accounts for geometric attenuation and shadowing, *i.e.* large-scale fading [20]. The transmitted signals in (1) are narrow in comparison to the total channel bandwidth, so it is natural to assume they will undergo flat Rayleigh fading. This means that the elements $h_{m,k}$ of the $M \times K$ channel matrix

$$\mathbf{H} = \underbrace{\begin{pmatrix} g_{1,1} & \cdots & g_{1,K} \\ \vdots & \ddots & \vdots \\ g_{M,1} & \cdots & g_{M,K} \end{pmatrix}}_{\mathbf{G}} \cdot \underbrace{\begin{pmatrix} d_1 & & \\ & \ddots & \\ & & d_K \end{pmatrix}^{1/2}}_{\mathbf{D}} \tag{3}$$

correspond to the complex channel gains from the transmit antennas to the receive antennas. The large-scale fading coefficients are assumed the same for $m = 1, \ldots, M$ BS antennas but dependent of the individual positions of MTC devices.

Under the assumption of large M and that small-scale fading coefficients experienced by each MTC device are i.i.d. random variables with zero mean and unit variance, the column channel vector from different MTC devices becomes asymptotically orthogonal as the number of receive antennas at the BS grows without bound [20]

$$\mathbf{H}^{\dagger}\mathbf{H} = \mathbf{D}^{1/2}\,\mathbf{G}^{\dagger}\mathbf{G}\,\mathbf{D}^{1/2} \approx M\mathbf{D}^{1/2}\mathbf{I}_K\mathbf{D}^{1/2} = M\mathbf{D}, \quad (4)$$

where $(\cdot)^{\dagger}$ denotes transpose-conjugate (Hermitian) operation. Please note that the *favorable propagation* condition shown in (4) is only valid in the context of Massive MIMO [70]. We refer the reader to [71] for a discussion on this condition, and to [22] for some fresh experimental evidence supporting the assumption of i.i.d. small-scale fading coefficients in Massive MIMO.

The vector received at the BS can be written as [25, 70]

$$\mathbf{y} = \sqrt{\rho}\,\mathbf{H}\,\mathbf{x} + \mathbf{n}, \quad (5)$$

where ρ is the uplink transmit power, $\mathbf{y} \in \mathbb{C}^{M\times 1}$, and $\mathbf{n} \in \mathbb{C}^{M\times 1}$ is a zero-mean noise vector with complex Gaussian distribution and identity covariance matrix. There exist M PNSCH signal versions in (5) for each of the K MTC devices. Hence, the task of the BS consists of detecting K simultaneous MTC transmissions on the basis of estimates of the channel coefficients in (3). Detection techniques need to be employed in order to separate each of the data streams transmitted by the various devices in a Massive MU-MIMO system.

We consider the case of perfect CSI, *i.e.* $\mathbf{H}$ is perfectly known at the BS. Let $\mathbf{A}$ be an $M \times K$ linear detector matrix that depends on the channel $\mathbf{H}$. By using a linear detector, the received signal can be separated into different data streams using $\mathbf{A}^{\dagger}$ as follows

$$\mathbf{r} = \mathbf{A}^{\dagger}\mathbf{y}, \quad (6)$$

where the vector $\mathbf{r}$ collects the data streams received at the BS, *i.e.* the OFDM symbols of all K single-antenna MTC devices, and $\mathbf{A}$ is a receive matrix that depends on the specific linear detector used at the BS. After linear detection, as seen in Figure 1, each data stream undergoes FFT processing and subcarrier extraction in order to retrieve data symbols.

Inspection of (3) reveals that $\mathbf{D}$ is a diagonal matrix, so we can use MRC in the uplink to separate the signals from different MTC devices into different streams with asymptotic no inter-user interference [20]. Thereby each MTC device's transmission can be seen as signals of a single device passing through a single input single output channel. In the limit, this implies that MRC is optimal when the number of receive antennas is much larger than the number of transmit antennas, *i.e.* $M \gg K$, $M \to \infty$ – as can be seen from (4). In MRC the linear detection matrix $\mathbf{A}$ is chosen using

$$\mathbf{A}_{\mathrm{MRC}} = \mathbf{H} \quad (7)$$

where the dominant computation is due to matrix transposition. The associated complexity is of only $\mathcal{O}(MK)$ multiplications.

ZF is an alternative linear filtering method that chooses $\mathbf{A}$ with the aim of completely eliminating interference, regardless of noise enhancement. Specifically, the ZF detector chooses $\mathbf{A}$ constrained to $\mathbf{AH} = \mathbf{I}$

$$\mathbf{A}_{\mathrm{ZF}} = \mathbf{H}(\mathbf{H}^{\dagger}\mathbf{H})^{-1}, \quad (8)$$

which is of complexity $\mathcal{O}(MK + MK^2 + K^3)$ [22]. One drawback of ZF is that it insists in forcing interference to zero independent of the interference strength, *i.e.* any energy of the signal of interest that lies in the interference subspace is discarded. A better strategy is to choose $\mathbf{A}$ so as to balance the signal energy lost with the increased interference. From this point of view, it is better to accept some residual interference provided that this allows the detector to capture more of the desired signal's energy [49].

One last linear detector that, together with MRC and ZF, poses complexity costs that do not depend on the modulation order is MMSE. As the name suggests, the MMSE detector chooses the $\mathbf{A}$ that minimizes $e = E[\|\mathbf{A}^{\dagger}\mathbf{y} - \mathbf{x}\|^2]$ without any additional constraints

$$\mathbf{A}_{\mathrm{MMSE}} = \mathbf{H}\left(\mathbf{H}^{\dagger}\mathbf{H} + \frac{\sigma_n^2}{\sigma_x^2}\mathbf{I}\right)^{-1}, \quad (9)$$

where σ_x^2 and σ_n^2 denote the variances of transmitted signal vector and noise vector, respectively. In contrast to ZF, which minimizes interference but fails to treat noise, and to MRC, which minimizes noise but fails to treat interference, MMSE achieves an optimal balance between interference suppression and noise enhancement at the same cost of ZF [22, 72].

The shortcomings listed in Table 1 under iterative filtering, random step search, and tree-based methods suggest that these detection classes perform well but are still too complex to be practical. Linear filtering methods, such as MRC, ZF, and MMSE, seem more feasible candidates for Massive MU-MIMO systems. For $1 \ll K \ll M$, it is known that linear detection performs fairly well, and asymptotically achieves capacity when $M \to \infty$. [20]. We therefore consider only such linear methods in the simulation work that follows.

4.2. Simulation Results

In this section, we assess the performances of MRC, ZF, and MMSE in terms of their Bit Error Rate (BER) over

a range of SINRs. As benchmark in the comparisons we use the Matched Filter Bound (MFB), also known in the literature as the perfect interference-cancellation bound. As the name suggests, MFB performs as the i-th user of a matched-filter receiver in the absence of other sources of interference [49]. Our motivation for this choice is that for $M \gg K$ both multi-user interference and small-scale fading effects tend to disappear (thanks to the large processing gains of Massive MIMO), so the performance of the MU-MIMO $K \times M$ channel (assumed to be flat Rayleigh fading in Section IV.A) becomes very close to the MFB.

In our simulation work, we consider uncoded QPSK/OFDM uplink block transmission with the number of FFT bins and the number of samples used to create the CP set up to $N = 2048$ and $N_{\mathrm{CP}} = 128$, respectively. The Massive MU-MIMO $K \times M$ channel is a flat Rayleigh fading channel. Each single path linking an MTC device to a receive antenna at the BS is modeled as a one-tap finite impulse response filter with a complex coefficient drawn from a zero-mean and unit variance Gaussian random process. Each path is assumed uncorrelated with the other paths.

The simulation results discussed in the sequel were averaged over 10^7 OFDM symbol realizations, with one channel realization (fading plus additive Gaussian white noise) per generated OFDM symbol. The simulation type is Monte-Carlo with a bit error counting procedure that compares the transmit bit vector (mapped into a transmitted OFDM symbol) to the receive bit vector (demapped from the received OFDM symbol).

Figure 2 shows the BER of linear filtering detectors for a fixed number of $K = 10$ MTC devices and BS array sizes in the range of $50 \leq M \leq 500$ antennas. The performance gap inherent to MRC becomes evident in this figure, although it can be dramatically reduced at the expense of larger array sizes at the BS, *e.g.* only 2 dB @BER $= 10^6$ for $M = 500$. This suggests that even low-complex MRC has potential to approximate MFB in case M can be made large enough.

As expected, and due to its better balance between interference suppression and noise enhancement, MMSE outperforms MRC and ZF in all cases studied. The performance gap between ZF and MMSE, which is small enough to be considered negligible for $M \leq 50$, entirely vanishes as the BS array size is grown to $M = 100$ or above. In fact, the main conclusion drawn from the plots is that MRC, ZF, and MMSE all approach the performance of MFB as M grows without bound, but the gap between the perfect interference-cancellation bound and ZF/MMSE decreases at a faster pace than in case of MRC.

5. Study Case II: FBMC-based Massive MIMO Networks

Networks resulting from the combination of Massive MIMO and FBMC are of the utmost importance as in these systems spectrum not only can be reused by all the users (advantage of Massive MIMO), but can also be used in an efficient manner (due to the FBMC's low OOB emissions). The application of FBMC to Massive MIMO was first considered in [24], with an interesting finding of this work being the *self-equalization* property of FBMC in Massive MIMO channels (in contrast with the limited applicability of FBMC to conventional MIMO channels). As a result, FBMC can leverage various benefits that place it in a strong position as a candidate for 5G systems.

Linear combining of the signals received in different receive antennas at BS averages channel distortions between the users and BS antennas. As M increases, the channel distortions over each subcarrier are smoothed through linear combining, so a nearly equalized gain across each subcarrier can be achieved. Assuming a flat channel over each subcarrier, we derived analytical SINR relationships for MF and MMSE combiners in [24]. We repeat such expressions in Section 5.1 for self-containment, and since they are used as benchmark to evaluate channel flatness in Section 5.2.

As recently highlighted in [74], Cosine Modulated Multitone (CMT), *viz.* a particular FBMC form, possesses a blind equalization capability [75] that can be used to decontaminate erroneous channel estimates caused by pilot contamination in multicellular Massive MIMO networks. This approach, which is somewhat similar to the Godard blind equalization algorithm [76], can be easily extended from single antenna to Massive MIMO systems. We will discuss this further in sections 5.1 and 5.2.

5.1. System Model

CMT-based Massive MIMO Networks. Consider a multi-cellular network consisting of $C > 1$ cells and K UEs in each cell. Each UE is equipped with a single transmit and receive antenna, communicating with the BS in a TDD manner. Each BS is equipped with $M \gg K$ transmit/receive antennas used to communicate with the K UEs in the cell *simultaneously*. We also assume, similar to [20], multicarrier modulation is used for data transmission. However, we replace OFDM modulation by CMT modulation. Each UE is distinguished by the BS using the respective subcarrier gains between its antenna and the BS antennas.

Ignoring time and subcarrier indices in our formulation, for ease of notation, a transmit symbol $s_c(\ell)$ from the ℓ^{th} UE located in the c^{th} cell, arrives at the j^{th} BS as a vector

$$\mathbf{x}_{j\ell} = t_c(\ell)\mathbf{h}_{cj\ell}, \tag{10}$$

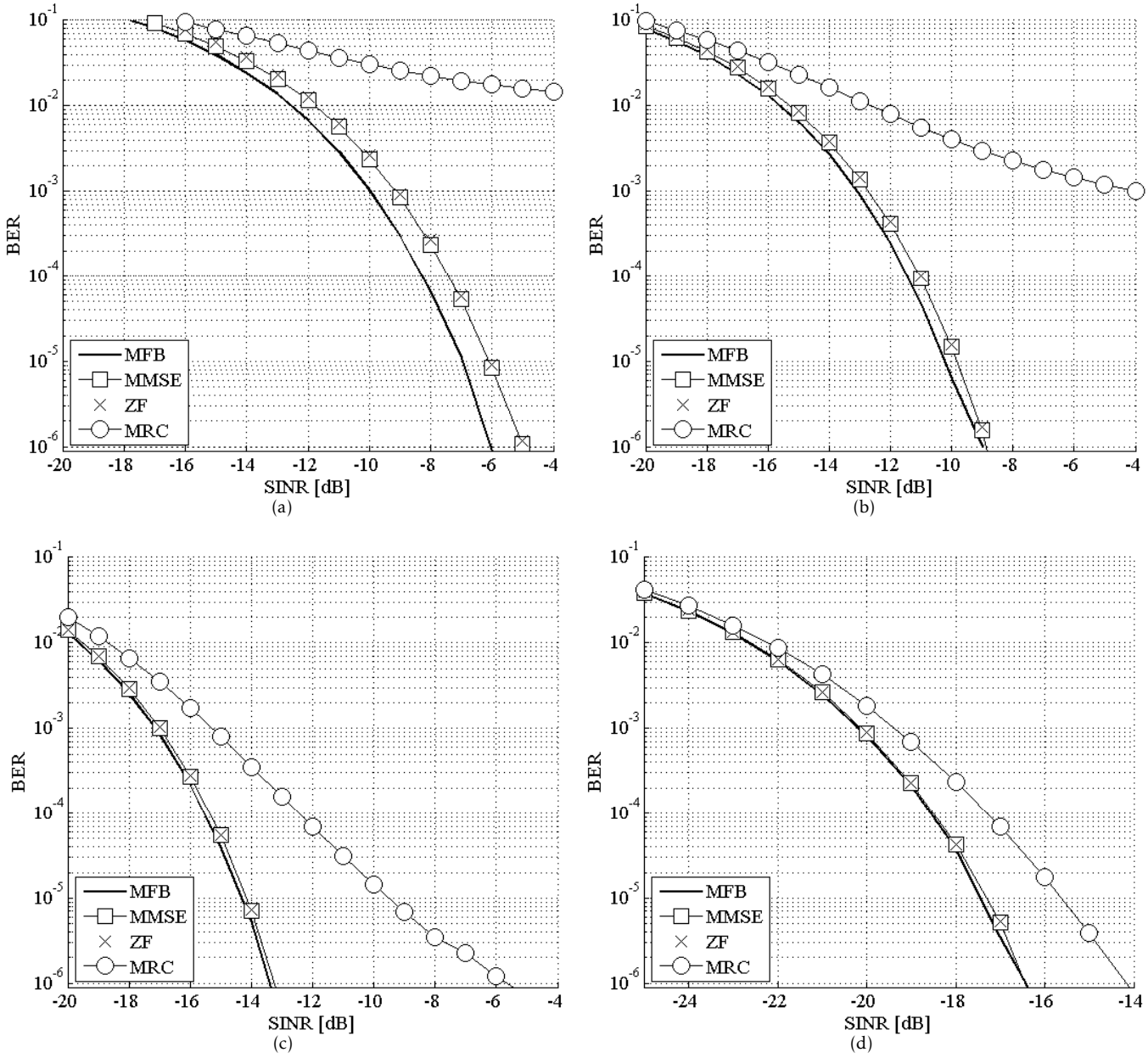

Figure 2. Results for Study Case I: BER performance of different linear filtering methods for $K = 10$ single-antenna MTC devices and different array sizes at the BS. MTB is provided as benchmark for comparisons. (a) $M = 50$ antennas. (b) $M = 100$ antennas. (c) $M = 250$ antennas. (d) $M = 500$ antennas.

where $t_c(\ell) = s_c(\ell) + jq_c(\ell)$ and $q_c(\ell)$ is the contribution of ISI and ICI. $\mathbf{h}_{cj\ell} = [h_{cj\ell}(0), \ldots, h_{cj\ell}(M-1)]^{\mathrm{T}}$ indicates the channel gain vector whose elements are the gains between the ℓ^{th} UE located in the c^{th} cell and different antennas at the j^{th} BS. The received signal vector at the j^{th} BS, $\mathbf{x}_j$, contains contributions from its own UEs and the ones located in its neighboring cells apart from the channel noise vector $\mathbf{v}$

$$\mathbf{x}_j = \sum_{c=0}^{C-1} \sum_{\ell=0}^{K-1} \alpha_{cj\ell} \mathbf{x}_{c\ell} + \mathbf{v}, \tag{11}$$

where $\alpha_{cj\ell}$'s are the cross-gain factors between the ℓ^{th} user of the c^{th} cell and the BS antennas of the j^{th} cell which can be thought as path loss coefficients. In general, $\alpha_{cj\ell} \in [0, 1]$. Considering perfect power control for the users of each cell implies that $\alpha_{cj\ell} = 1$ for $c = j$. The vector $\mathbf{x}_j$ is fed into a set of linear estimators at the j^{th} BS to estimate the users' data symbols $s_j(0), s_j(1), \cdots, s_j(K-1)$. (11) can then be rearranged as

$$\mathbf{x}_j = \mathbf{H}_{jj}\mathbf{t}_j + \sum_{\substack{c=0 \\ c\neq j}}^{C-1} \mathbf{H}_{cj}\boldsymbol{\alpha}_{cj}\mathbf{t}_c + \mathbf{v}, \tag{12}$$

where $\mathbf{t}_c = [t_c(0), \ldots, t_c(K-1)]^{\mathrm{T}}$ and $\boldsymbol{\alpha}_{cj} = \mathrm{diag}\{\alpha_{cj0}, \ldots, \alpha_{cj(K-1)}\}$. The $\mathbf{H}_{cj}$'s are $M \times K$ fast fading channel matrices with columns $\mathbf{h}_{cj\ell}$, $\ell = 0, 1, \ldots, K-1$.

To cast the above process in a mathematical formulation for the single cell case, and allow the introduction of various choices of estimators, we proceed as follows. First, define $\tilde{\mathbf{x}} = [\mathbf{x}_{\mathrm{R}}^{\mathrm{T}}\ \mathbf{x}_{\mathrm{I}}^{\mathrm{T}}]^{\mathrm{T}}$, $\tilde{\mathbf{v}} = [\mathbf{v}_{\mathrm{R}}^{\mathrm{T}}\ \mathbf{v}_{\mathrm{I}}^{\mathrm{T}}]^{\mathrm{T}}$, $\tilde{\mathbf{h}}_\ell = [\mathbf{h}_{\ell,\mathrm{R}}^{\mathrm{T}}\ \mathbf{h}_{\ell,\mathrm{I}}^{\mathrm{T}}]^{\mathrm{T}}$, $\check{\mathbf{h}}_\ell = [-\mathbf{h}_{\ell,\mathrm{I}}^{\mathrm{T}}\ \mathbf{h}_{\ell,\mathrm{R}}^{\mathrm{T}}]^{\mathrm{T}}$, $\mathbf{s} = [s(0)\ s(1)\ \cdots\ s(K-1)]^{\mathrm{T}}$ and $\mathbf{q} = [q(0)\ q(1)\ \cdots\ q(K-1)]^{\mathrm{T}}$, where the subscripts 'R' and 'I' denote the real and imaginary parts, respectively. Using these definitions, (11) may then be rearranged as

$$\tilde{\mathbf{x}} = \mathbf{A}\begin{bmatrix} \mathbf{s} \\ \mathbf{q} \end{bmatrix} + \tilde{\mathbf{v}}, \tag{13}$$

where $\mathbf{A} = [\tilde{\mathbf{H}}\ \check{\mathbf{H}}]$, and $\tilde{\mathbf{H}}$ and $\check{\mathbf{H}}$ are $2M \times K$ matrices with columns of $\{\tilde{\mathbf{h}}_\ell,\ \ell = 0, 1, \cdots, K-1\}$ and $\{\check{\mathbf{h}}_\ell,\ \ell = 0, 1, \cdots, K-1\}$, respectively. The form of (13) is familiar in the Code Division Multiple Access (CDMA) literature (see, *e.g.* [77, 78]), hence, a variety of solutions that have been given for CDMA systems can be immediately applied to the present problem as well.

For instance, the MF detector obtains an estimate of the vector $\mathbf{s}$ using

$$\hat{\mathbf{s}}_{\mathrm{MF}} = \mathbf{D}^{-1}\boldsymbol{\Gamma}\mathbf{A}^{\mathrm{T}}\tilde{\mathbf{x}}, \tag{14}$$

where $\mathbf{D} = \mathrm{diag}\{\|\tilde{\mathbf{h}}_0\|^2, \ldots, \|\tilde{\mathbf{h}}_{K-1}\|^2\}$, the matrix $\boldsymbol{\Gamma}$ consists of the first K rows of the identity matrix $\mathbf{I}_{2K}$ and $\hat{\mathbf{s}}_{\mathrm{MF}} = [\hat{s}_{\mathrm{MF}}(0), \ldots, \hat{s}_{\mathrm{MF}}(K-1)]^{\mathrm{T}}$ whose ℓ^{th} element, $\hat{s}_{\mathrm{MF}}(\ell)$, is the estimated data symbol of user ℓ. Each element of $\hat{\mathbf{s}}_{\mathrm{MF}}$ can be expanded as

$$\hat{s}_{\mathrm{MF}}(\ell) = s(\ell) + \sum_{\substack{i=0 \\ i\neq\ell}}^{K-1} \frac{\tilde{\mathbf{h}}_\ell^{\mathrm{T}}}{\|\tilde{\mathbf{h}}_\ell\|^2}(\tilde{\mathbf{h}}_i s(i) + \check{\mathbf{h}}_i q(i)) + \frac{\tilde{\mathbf{h}}_\ell^{\mathrm{T}}}{\|\tilde{\mathbf{h}}_\ell\|^2}\tilde{\mathbf{v}}. \tag{15}$$

This leads to a receiver structure similar to that of [20], where it is shown that when the number of antennas, M, increases to infinity, the multiuser interference and noise effects vanish to zero. Hence, $\hat{\mathbf{s}} = \mathbf{s}$, where the vector $\hat{\mathbf{s}}$ is an estimate of $\mathbf{s}$, and the receiver will be optimum. In the context of CDMA, this has the explanation that as M tends to infinity, the processing gain also goes to infinity and accordingly multiuser interference and noise effects vanish.

In realistic situations when M is finite, the MF estimator is not optimal. A superior estimator is MMSE

$$\hat{\mathbf{s}} = \mathbf{W}^{\mathrm{T}}\tilde{\mathbf{x}}, \tag{16}$$

where the coefficient matrix $\mathbf{W}$ is chosen to minimize the cost function

$$\zeta = \mathbb{E}[\|\mathbf{s} - \mathbf{W}^{\mathrm{T}}\tilde{\mathbf{x}}\|^2]. \tag{17}$$

This solution is optimal in that it maximizes the SINR [77]. Following standard derivations, the optimal choice of $\mathbf{W}$ is

$$\mathbf{W}_{\mathrm{o}} = \mathbf{A}\left(\mathbf{A}^{\mathrm{T}}\mathbf{A} + \sigma_v^2\mathbf{I}_{2K}\right)^{-1}\boldsymbol{\Gamma}^{\mathrm{T}} \tag{18}$$

where it is assumed that the elements of the noise vector $\tilde{\mathbf{v}}$ are i.i.d. Gaussian random variables with variances of σ_v^2, so $\mathbb{E}\left[\tilde{\mathbf{v}}\tilde{\mathbf{v}}^{\mathrm{T}}\right] = \sigma_v^2\mathbf{I}$. The columns of $\mathbf{W}_{\mathrm{o}}$ contain the optimal filter tap weights for different users. Plugging (18) into (16) leads to the MMSE solution

$$\begin{aligned}\hat{s}_{\mathrm{MMSE}}(\ell) \quad = \quad & \mathbf{w}_{\mathrm{o},\ell}^{\mathrm{T}}\tilde{\mathbf{h}}_\ell s(\ell) + \sum_{\substack{i=0 \\ i\neq\ell}}^{K-1} \mathbf{w}_{\mathrm{o},\ell}^{\mathrm{T}}\tilde{\mathbf{h}}_i s(i) \\ & + \sum_{i=0}^{K-1} \mathbf{w}_{\mathrm{o},\ell}^{\mathrm{T}}\check{\mathbf{h}}_i q(i) + \mathbf{w}_{\mathrm{o},\ell}^{\mathrm{T}}\tilde{\mathbf{v}},\end{aligned} \tag{19}$$

where $\mathbf{w}_{\mathrm{o},\ell}$ is the ℓ^{th} column of $\mathbf{W}_{\mathrm{o}}$. Ignoring the off-diagonal elements of $\left(\mathbf{A}^{\mathrm{T}}\mathbf{A} + \sigma_v^2\mathbf{I}_{2K}\right)$ and removing the term $\sigma_v^2\mathbf{I}_{2K}$ from (18), one will realize that (19) boils down to the MF tap weights (15).

The first terms on the right hand side of (15) and (19) are the desired signal and the rest are the interference plus noise terms. We consider $s(\ell)$ and $q(\ell)$ as independent variables with variance of unity. Under the assumption of a flat channel impulse response in each subcarrier band, the SINR at the output of MF and MMSE detectors for user ℓ in a certain subcarrier can respectively be derived as

$$\mathrm{SINR}_{\mathrm{MF}}(\ell) = \frac{\|\tilde{\mathbf{h}}_\ell\|^4}{\sum_{\substack{i=0 \\ i\neq\ell}}^{K-1}\left(|\tilde{\mathbf{h}}_\ell^{\mathrm{T}}\tilde{\mathbf{h}}_i|^2 + |\tilde{\mathbf{h}}_\ell^{\mathrm{T}}\check{\mathbf{h}}_i|^2\right) + \sigma_v^2\|\tilde{\mathbf{h}}_\ell\|^2}, \tag{20}$$

and

$$\mathrm{SINR}_{\mathrm{MMSE}}(\ell) = \frac{|\mathbf{w}_{\mathrm{o},\ell}^{\mathrm{T}}\tilde{\mathbf{h}}_\ell|^2}{\sum_{\substack{i=0 \\ i\neq\ell}}^{K-1}|\mathbf{w}_{\mathrm{o},\ell}^{\mathrm{T}}\tilde{\mathbf{h}}_i|^2 + \sum_{i=0}^{K-1}|\mathbf{w}_{\mathrm{o},\ell}^{\mathrm{T}}\check{\mathbf{h}}_i|^2 + \sigma_v^2\|\mathbf{w}_{\mathrm{o},\ell}\|^2}. \tag{21}$$

Pilot Decontamination. Consider now the multi-cellular scenario whose general system model has already been introduced in Section 5.1. Under the assumption of perfect CSI, the MF tap-weight vector for user ℓ located in the j^{th} cell can be represented as

$$\mathbf{w}_{j\ell} = \frac{\mathbf{h}_{jj\ell}}{\mathbf{h}_{jj\ell}^{\mathrm{H}}\mathbf{h}_{jj\ell}}. \tag{22}$$

The estimated users' data symbols at the output of the matched filters of the cell j can be mathematically written as

$$\hat{\mathbf{s}}_j = \Re\mathfrak{e}\{\mathbf{D}^{-1}\mathbf{H}_{jj}^{\mathrm{H}}\mathbf{x}_j\}, \tag{23}$$

where $\mathbf{D} = \mathrm{diag}\{\|\mathbf{h}_{jj0}\|^2, \ldots, \|\mathbf{h}_{jj(K-1)}\|^2\}$ and $\hat{\mathbf{s}}_j$ is the estimation of the vector $\mathbf{s}_j = [s_j(0), \ldots, s_j(K-1)]^{\mathrm{T}}$ which contains the users' transmitted data symbols. In practical situations where M is finite, the MF combiner is not optimal and as it is pointed out in [24], MMSE combining has a superior performance which is due to the fact that it maximizes the SINR.

The channel gains between the UEs and the BS antennas in each cell are estimated through training pilots transmitted during the uplink phase. The UEs in each cell transmit pilots from a set of mutually orthogonal pilot sequences which allows the BS to distinguish between the channel impulse responses of different users in the channel estimation stage. As argued in [73], the channel coherence time does not allow the users of neighboring cells to use orthogonal pilot sequences in the multi-cellular scenario.

In TDD multi-cellular Massive MIMO networks, C BSs use the same set of pilot sequences as well as frequencies. In addition, synchronous transmissions are assumed. Therefore, the same set of pilot sequences being used in neighboring cells will adversely affect the channel estimates at the BS. This effect is called pilot contamination. After correlating the received training symbols with the set of pilot sequences at the BS j, the estimates of the channel gains between the UEs and large antenna array of the BS can be given as

$$\hat{\mathbf{H}}_{jj} = \mathbf{H}_{jj} + \sum_{\substack{c=0 \\ c\neq j}}^{C-1} \mathbf{H}_{cj}\boldsymbol{\alpha}_{cj} + \tilde{\mathbf{v}}. \tag{24}$$

As one can realize from (24), the channel estimates at the j^{th} cell are corrupted by the channel impulse responses of its adjacent cells. Therefore, even with infinite number of receive antennas at the BS, there will always exist some multiuser interference from the users of other cells. Pilot contamination can have detrimental effects on the performance of multi-cellular networks and greatly impair their sum rate capacity [20]. Here we extend the blind equalization property of CMT to Massive MIMO systems in order to purify the channel estimates and tackle the pilot contamination problem without any need for cooperation among the cells or additional training information.

As it is noted in [75], the imaginary part of the CMT symbol at each subcarrier, *i.e.* $q_c(\ell)$, is formed from a linear combination of a large number of symbols from the corresponding and also adjacent subcarriers. Following the central limit theorem, one can come up with three observations here:

1. The favorable real-part of the equalized CMT symbol at each subcarrier is free of ISI and ICI and, as such, its distribution follows that of the respective Pulse Amplitude Modulation (PAM) alphabet.
2. The respective imaginary part suffers from ISI and ICI and is distributed in a Gaussian manner.
3. Both the real and imaginary parts of an unequalized symbol at a subcarrier comprise of ISI and ICI terms and are distributed in a Gaussian manner.

Based on the aforementioned properties, a blind equalization algorithm similar to the Godard blind equalization algorithm [76] was developed in [75] such that the cost function

$$\xi = \mathbb{E}[(|y_k(n)|^p - R)^2], \tag{25}$$

is minimized. $y_k(n)$ is the equalizer output (in the case here, the equalizer output of the k^{th} subcarrier channel), p is integer (usually set equal to 1 or 2), $R = \mathbb{E}[|s|^{2p}]/\mathbb{E}[|s|^p]$, and s is a random selection from the PAM symbols alphabet.

We shall now devise a strategy to exploit this algorithm in order to adaptively correct the imperfect channel estimates and hence greatly alleviate the performance degradation due to the contaminated pilots. A Least Mean Squares (LMS)-like blind-tracking algorithm, which is computationally inexpensive, based on the cost function (25) can be adopted. Extension of the proposed blind equalization technique of [75] to Massive MIMO application can be straightforwardly derived as

$$\mathbf{w}_{j\ell}(n+1) = \mathbf{w}_{j\ell}(n) - 2\mu\,\mathrm{sign}(\hat{s}_j^{(n)}(\ell))(|\hat{s}_j^{(n)}(\ell)| - R)\cdot\mathbf{x}_j(n), \tag{26}$$

where $\hat{s}_j^{(n)}(\ell) = \mathbf{w}_{j\ell}^{\mathrm{H}}(n)\mathbf{x}_j(n)$, $\mathbf{x}_j(n)$ is the n^{th} symbol of the received data packet and μ is an step-size parameter. We initialize the algorithm through the MF tap-weight vector

$$\mathbf{w}_{j\ell}^{(0)} = \frac{\hat{\mathbf{h}}_{jj\ell}}{\hat{\mathbf{h}}_{jj\ell}^{\mathrm{H}}\hat{\mathbf{h}}_{jj\ell}}, \tag{27}$$

where $\hat{\mathbf{h}}_{jj\ell}$ is the estimated channel vector between the user ℓ located in the cell j and the j^{th} BS antenna arrays, *i.e.* the ℓ^{th} column of $\hat{\mathbf{H}}_{jj}$ in (24).

In Section 5.2 we will show through numerical results that our channel tracking algorithm is able to effectively converge towards the MMSE linear combining with perfect knowledge of channel responses of all users in all considered cells, while starting from MF tap-weights with imperfect CSI. Although originally presented in [24] and [74], these results are reproduced here for the sake of self-containment.

5.2. Simulation Results

CMT-based Massive MIMO Networks. Figure 3(a) shows theoretical and simulation results of a multi-user scenario ($K = 6$ users, $L = 64$ subcarriers, and $M = 128$ BS antennas). The target output SINR of 20 dB may be calculated as $\text{SNR}_{\text{in}} + 10\log_{10} M$, where SNR_{in} is the signal-to-noise ratio at each BS antenna, and $10\log_{10} M$ is the spreading gain due to M BS antennas. SINRs are evaluated over all subcarrier channels, and the number of points along the normalized frequency is equal to the number of subcarrier bands, L. MMSE is superior to MF, and its SINR is about the same for all subcarriers, *i.e.* has smaller variance across the subcarriers. Our simulation results match very well to the theoretical ones, confirming the self-equalization property of linear combining in FBMC-based Massive MIMO systems.

This self-equalization property of FBMC relaxes the large L requirement to obtain an approximately flat gain over each subcarrier band, so wider subcarriers can be used. The use of a smaller L in a given bandwidth: (1) reduces the latency caused by synthesis/analysis filter banks; (2) improves bandwidth efficiency due to the absence of the CP and to shorter preambles; (3) decreases computational complexity due to the smaller FFT and IFFT blocks needed for implementation; (4) provides robustness to frequency offsets; and (5) reduces PAPR.

Pilot Decontamination. To alleviate the performance loss caused by corrupted channel estimates, the blind equalization technique adaptively corrects the linear combiner tap weights. Starting with MF using noisy channel estimates, the SINR performance reaches that of MF with noise-free channel matrix within a small number of iterations, and keeps improving to get to that of MMSE with noise-free channel matrix.

This is shown in Figure 3(b) for a Massive MIMO network in TDD mode with seven cells and one user per cell. We assume that all users use the same pilot sequences, and that $L = 256$ and $M = 128$. It can be seen that there is an abrupt SINR improvement during the first 50 iterations where the output SINR of the blind combiner reaches that of the MF combiner with the perfect CSI knowledge. Running larger numbers of iterations has shown that the output SINR of our blind channel tracking technique can suppress the pilot contamination effect and converge towards that of the MMSE combiner. Apart from its high computational complexity, the MMSE detector needs perfect knowledge of the channel impulse responses between the interfering users of the other cells and its antenna arrays – a rather unrealistic condition. The methods proposed here, on the other hand, can approach MMSE performance with a simple LMS-like algorithm.

In some situations where the length of the UL data packets is close to the channel coherence time, the estimated CSI in the beginning of the packet may get outdated, resulting in a performance loss (as the same CSI is used for precoding in the DL). This problem can be alleviated by the utilization of blind channel tracking techniques as the one mentioned above, since these provide up-to-date CSI. In other words, the blind channel tracking techniques sweep through all the symbols in the data packet and update the CSI. The latest CSI taken from the last transmitted symbols can thus be obtained.

6. Concluding Remarks

This article has reviewed existing related work and identified main issues and candidate solutions in the key area of Massive MIMO systems. We have illustrated the crucial role this technology is envisioned to play in the context of 5G wireless communication systems by means of the following study cases.

In the first study case, we propose the use of a Massive MU-MIMO setup as means to tackle the uplink mixed-service communication problem. Our simulation results suggest that, as the size of the antenna array at the BS is made progressively larger, the performances of sub-optimal linear filtering methods approach the perfect interference-cancellation bound. ZF and MMSE approach the MFB at faster pace than simple MRC, although the performance gap of the latter is of only 2 dB for $M = 500$ antennas. Due to its better balance between interference suppression and noise enhancement, MMSE outperforms MRC and ZF in all cases studied. The gap in the performance of ZF, however, is negligible for array sizes around 50 antennas, and entirely vanishes for $M \geq 100$ antennas.

Our second study case looks at the intersection of Massive MIMO and waveform design. Here we have introduced the property of self-equalization FBMC-based Massive MIMO networks, and show that it has potential to reduce the number of subcarriers required by the system. It is also shown that the blind channel tracking property of FBMC can be used to address pilot contamination – one of the main performance limiting factors of Massive MIMO systems.

The findings presented in this paper shed light into and motivate for two entirely new research lines towards a better understanding of Massive MU-MIMO for MTC networks and FBMC-based Massive MIMO networks. In our future work, we will consider more realistic channel models and relax the assumption of perfect channel knowledge on the part of the BS. We also intend to extend our analysis with robust design linear filters, being thus able to compare their performance to that obtained in this paper for standard MRC, ZF, and MMSE.

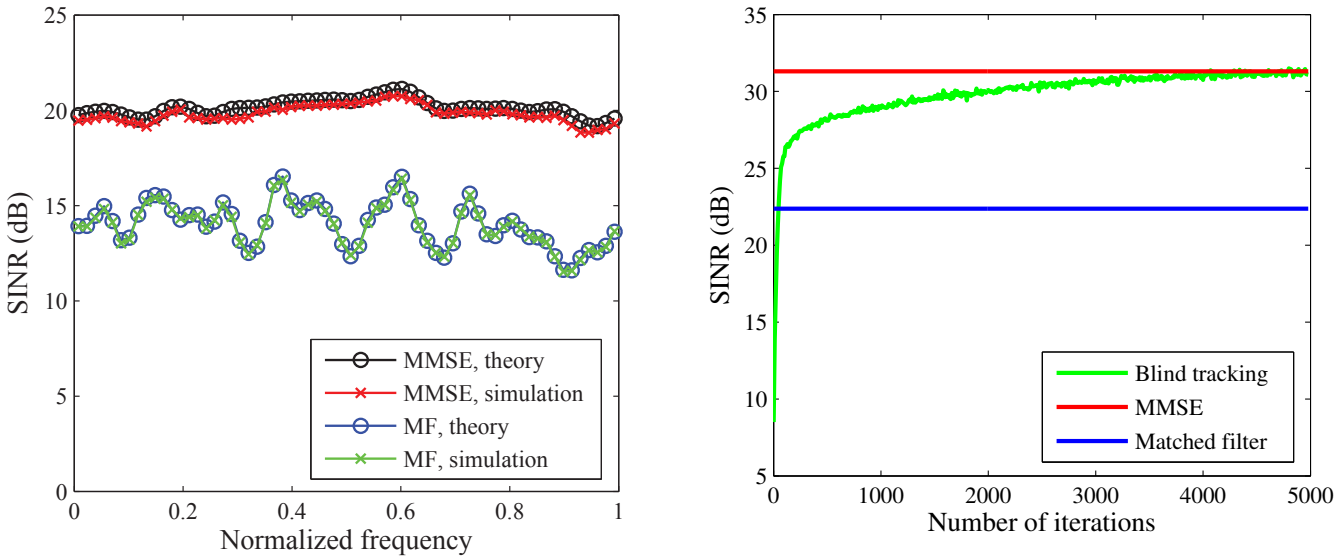

Figure 3. Results for Study Case II: SINR performance of different linear combiners for the case of $M = 128$ antennas at the BS. (a) MMSE *vs.* MF ($L = 64$ subcarriers, $K = 6$ users). (b) Blind tracking technique *vs.* MMSE *vs.* MF ($L = 256$ subcarriers, $C = 7$ cells, $K = 1$ user per cell). These results were first presented in [24] and [74], and are reproduced here for self-containment.

References

[1] 4G Americas White Papers. 4G Americas' Recommendations on 5G Requirements and Solutions. http://www.4gamericas.org/en/resources/white-papers/ (acessed on 19 March 2015).

[2] Fettweis, G. and Alamouti, S. (2014) 5G: Personal Mobile Internet beyond What Cellular Did to Telephony. *IEEE Commun. Mag.*, **52**(2): 140-145.

[3] Wunder, G. et al. (2014) 5GNOW: Non-Orthogonal Asynchronous Waveforms for Future Mobile Applications. *IEEE Commun. Mag.*, **52**(2): 97-105.

[4] Boswarthick, D., Elloumi, O. and Hersent, O. (2012) *M2M Communications: A Systems Approach* (Wiley).

[5] Elmangoush, A. et al. (2012) Promoting M2M Application Development for Smart City. In *Proceedings of the 129th Meeting of the Wireless World Research Forum*.

[6] Corchado, J. M. et al. (2009) Using Heterogeneous Wireless Sensor Networks in a Telemonitoring System for Healthcare. *IEEE Trans. Inf. Technol. Biomed.*, **14**(2): 234-240.

[7] Papadimitratos, P. et al. (2009) Vehicular Communication Systems: Enabling Technologies, Applications, and Future Outlook on Intelligent Transportation, *IEEE Commun. Mag.*, **11**(1): 84-95.

[8] Moslehi, K. and Kumar, R. (2010) A reliability perspective of the smart grid, *IEEE Trans. Smart Grid*, **1**(1): 57-64.

[9] Kyriakides, E. and Polycarpou, M. (2015) *Intelligent Monitoring, Control and Security of Critical Infrastructure Systems* (Springer), 1st ed.

[10] Pattichis, C. S. et al. (2002) Wireless Telemedicine Systems: An Overview. *IEEE Antennas Propag. Mag.*, **44**(2): 143-153.

[11] Majerowicz, A. and Tracy, S. (2010) Telemedicine: Bridging Gaps in Healthcare Delivery. *Journal of AHIMA*, **81**(5): 52-53.

[12] Araniti, G. et al. (2013) LTE for Vehicular Networking: A Survey. *IEEE Commun. Mag.*, **51**(5): 148-157.

[13] ElBatt, T. et al. (2006) Cooperative Collision Warning using Dedicated Short Range Wireless Communications. In *Proceedings of the Int. Workshop Veh. Ad Hoc Networks*, pp. 1-9.

[14] Ide, C., Kurtz, F. and Wietfeld, C. (2013) Cluster-Based Vehicular Data Collection for Efficient LTE Machine-Type Communication. In *Proceedings of the IEEE VTC*, pp. 1-5.

[15] da Costa, F. (2014) *Rethinking the Internet of Things: A Scalable Approach to Connecting Everything* (Apress), 1st ed.

[16] Villaverde, B. C. et at. (2014) Service Discovery Protocols for Constrained Machine-to-Machine Communications. *IEEE Commun. Surveys Tuts.*, **16**(1): 41-60.

[17] Wunder, G., Kasparick, M. and Jung, P. (2015) Spline Waveforms and Interference Analysis for 5G Random Access with Short Message Support. *arXiv*:1501.02917

[18] Wunder, G., Jung, P. and Wang, C. (2014) Compressive Random Access for Post-LTE Systems. In *Proceedings of the IEEE ICC - Workshop on Massive Uncoordinated Access Protocols*, 539-544.

[19] Andrews, J.G. et al. (2014) What Will 5G Be? *IEEE J. Sel. Areas Commun.*, **32**(6): 1065-1082.

[20] Marzetta, T. L. (2010) Noncooperative Cellular Wireless with Unlimited Numbers of Base Station Antennas. *IEEE Trans. Wireless Commun.*, **9**(11): 3590-3600.

[21] Banelli, P. et al. (2014) Modulation Formats and Waveforms for the Physical Layer of 5G Wireless Networks: Who Will be the Heir of OFDM? *arXiv*:1407.5947
[22] Rusek, F. et al. (2013) Scaling Up MIMO: Opportunities and Challenges with Very Large Arrays. *IEEE Sig. Process. Mag.*, **30**(1): 40-60.
[23] Farhang-Boroujeny, B. (2011) OFDM Versus Filter Bank Multicarrier. *IEEE Sig. Process. Mag.*, **28**(3): 92-112.
[24] Farhang, A. et al. (2014) Filter Bank Multicarrier for Massive MIMO. In *Proceedings of the IEEE VTC*, 1-5.
[25] Larsson, E. G. et al. (2014) Massive MIMO for Next Generation Wireless Systems. *IEEE Commun. Mag.*, **52**(2): 186-195.
[26] Shepard, C. et al. (2012) Argos: Practical many-antenna base stations. In *Proceedings of the ACM MobiCom*, 53-64.
[27] Janaswamy, R. (2002) Effect of element mutual coupling on the capacity of fixed length linear arrays. *IEEE Antennas Wireless Propagat. Lett.*, **1**(1): 157-160.
[28] Wallace, J. W. and Jensen, M. A. (2004) Mutual coupling in MIMO wireless systems: A rigorous network theory analysis. *IEEE Trans. Wireless Commun.*, **3**(4): 1317-1325.
[29] Lau, B. K. et al. (2006) Impact of matching network on bandwidth of compact antenna arrays. *IEEE Trans. Antennas Propag.*, **54**(11): 3552-3238.
[30] Sibille, A., Oestges, C. and Zanella, A. (2010) *MIMO: From Theory to Implementation* (Academic Press).
[31] Artiga, X., Devillers, B. and Perruisseau-Carrier, J. (2014) On the selection of radiating elements for compact indoor massive-multiple input multiple output base stations. *IET Microw., Antennas & Propag.*, **8**(1): 1-9.
[32] Moustakas, A. L. et al. (2000) Communication through a diffusive medium: Coherence and capacity. *Science*, **287**: 287-290.
[33] Gao, X., Tufvesson, F. and Edfors, O. (2013) Massive MIMO channels - measurements and models. In *Proceedings of the Asilomar Conf. on Signals, Systems, and Computers*, 280-284.
[34] Zheng, K. Ou, S. and Yin, X. (2014) Massive MIMO Channel Models: A Survey. *Int. J. Antennas and Propag.*, **2014**: 10 pages.
[35] Jiang, Z. et al. (2014) Achievable Rates of FDD Massive MIMO Systems with Spatial Channel Correlation. *arXiv:1406.7486*
[36] Jose, J. et al. (2011) Pilot Contamination and Precoding in Multi-Cell TDD Systems. *IEEE Trans. Wireless Commun.*, **10**(8): 2640-2651.
[37] Kaltenberger, F. et al. (2010) Relative channel reciprocity calibration in MIMO/TDD systems. In *Proceedings of the Future Network and Mobile Summit*, 1-10.
[38] Rogalin, R. et al. (2013) Hardware-Impairment Compensation for Enabling Distributed Large-Scale MIMO. In *Proceedings of the Inf. Theory and Applicat. Workshop*, 1-10.
[39] Rogalin, R. et al. (2014) Scalable Synchronization and Reciprocity Calibration for Distributed Multiuser MIMO. *IEEE Trans. Wireless Commun.*, **13**(4): 1815-1831.
[40] Ngo, H. Q. and Larsson, E. G. (2012) EVD-based channel estimations for multicell multiuser MIMO with very large antenna arrays. In *Proceedings of the IEEE ICASSP*, 3249-3252.
[41] Ashikhmin, A. and Marzetta, T. L. (2012) Pilot contamination precoding in multi-cell large scale antenna systems. In *Proceedings of the IEEE ISIT*, 1137-1141.
[42] Yin, H. et al. (2013) A coordinated approach to channel estimation in large-scale multiple-antenna systems. *IEEE J. Sel. Areas Commun.*, **31**(2): 264-273.
[43] Mueller, R., Vehkaperae, M. and Cottatellucci, L. (2014) Blind Pilot Decontamination. *arXiv:1309.6806*
[44] de Lamare, R. C. (2013) Massive MIMO Systems: Signal Processing Challenges and Research Trends. *arXiv:1310.7282*
[45] Zu, K., de Lamare, R. C. and Haardt, M. (2013) Generalized design of low-complexity block diagonalization type precoding algorithms for multiuser MIMO systems. *IEEE Trans. Commun.*, **61**(10): 4232-4242.
[46] Caire, G. and Shamai, S. (2003) On the achievable throughput of a multiantenna Gaussian broadcast channel. *IEEE Trans. Inform. Theory*, **49**(7): 1691-1706.
[47] Windpassinger, C. et al. (2006) A performance study of MIMO detectors. *IEEE Trans. Wireless Commun.*, **5**(8): 2004-2008.
[48] Peel, C. B. et al. (2005) A vector-perturbation technique for near-capacity multiantenna communication, part I: Channel inversion and regularization. *IEEE Trans. Commun.*, **53**(1): 195-202.
[49] Barry, J. R., Lee, E. A. and Messerschmitt, D. G. (2004) *Digital Communication* (Springer), 3rd ed.
[50] Liang, Y. -C. et al. (2008) On the relationship between MMSE-SIC and BI-GDFE receivers for large multiple-input multiple-output channels. *IEEE Trans. Signal Process.*, **56**(8): 3627-3637.
[51] Zhao, H., Long, H. and Wang, W. (2007) Tabu search detection for MIMO systems. In *Proceedings of the IEEE PIMRC*, 1-5.
[52] Sun, Y. (2009) A family of likelihood ascent search multiuser detectors: An upper bound of bit error rate and a lower bound of asymptotic multiuser efficiency. *IEEE J. Sel. Areas Commun.*, **57**(6): 1743-1752.
[53] Jaldén, J. and Ottersten, B. (2005) On the complexity of sphere decoding in digital communications. *IEEE Trans. Signal Process.*, **53**(4): 1474-1484.
[54] Barbero, L. and Thompson, J. (2008) Fixing the complexity of the sphere decoder for MIMO detection. *IEEE Trans. Wireless Commun.*, **7**(6): 2131-2142.
[55] Loulou, A. E. and Renfors, M. (2013) Effective Schemes for OFDM Sidelobe Control in Fragmented Spectrum Use. In *Proceedings of the IEEE PIMRC*, 471-475.
[56] Berardinelli, G. et al. (2013) Zero-tail DFT-spread-OFDM signals. In *Proceedings of the IEEE Globecom*, 229-234.
[57] Berardinelli, G. et al. (2014) On the potential of OFDM enhancements as 5G waveforms. In *Proceedings the IEEE VTC*, 1-5.
[58] Renfors, M. et al. (2014) Analysis and Design of Efficient and Flexible Fast-Convolution Based Multirate Filter Banks. *IEEE Trans. Signal Process.*, **62**(15): 3768-3783.
[59] Kasparick, M. et al. (2014) Bi-orthogonal Waveforms for 5G Random Access with Short Message Support. In *Proceedings of the European Wireless Conference*, 293-298.

[60] Michailow, N. et al. (2014) Generalized Frequency Division Multiplexing for 5th Generation Cellular Networks. *IEEE Trans. Commun.*, **PP**(99): 18 pages.
[61] Datta, R. and Fettweis, G. (2014) Improved ACLR by Cancellation Carrier Insertion in GFDM based Cognitive Radios. In *Proceedings of the IEEE VTC*, 1-5.
[62] Aminjavaheri, A., Farhang, A., RezazadehReyhani, A., and Farhang-Boroujeny, B. (2015) Impact of Timing and Frequency Offsets on Multicarrier Waveform Candidates for 5G. *arXiv*:1505.00800
[63] Farhang, A., Marchetti, N., and Doyle, L. E. (2015) Low Complexity Transceiver Design for GFDM. *arXiv*:1501.02940
[64] Schaich, F. Wild, T. and Chen, Y. (2014) Waveform contenders for 5G - suitability for short packet and low latency transmissions. In *Proceedings of the IEEE VTC*, 1-5.
[65] Lien, S. -Y., Chen, K. -C. and Lin, Y. (2011) Toward Ubiquitous Massive Accesses in 3GPP Machine-to-machine Communications. *IEEE Commun. Mag.*, **49**(4): 66-74.
[66] Cheng, M.-Y. et al. (2012) Overload control for machine-type-communications in LTE-advanced system. *IEEE Commun. Mag.*, **50**(6): 38-45.
[67] Gerasimenko, M. et al. (2012) Energy and delay analysis of LTE-advanced RACH performance under MTC overload. In *Proceedings of the IEEE Globecom Workshops*, 1632-1637.
[68] Phuyal, U. et al. (2012) Controlling access overload and signaling congestion in M2M networks. In *Proceedings of the Asilomar Conference on Signals, Systems, and Computers*, 591-595.
[69] de Figueiredo, F. A. P. et al. (2013) Multi-stage Based Cross-Correlation Peak Detection for LTE Random Access Preambles. *Revista Telecomunicações*, **15**: 1-7.
[70] Ngo, H. Q., Larsson, E. G. and Marzetta, T. L. (2013) Energy and spectral efficiency of very large multiuser MIMO systems. *IEEE Trans. Commun.*, **61**(4): 1436-1449.
[71] Matthaiou, M. et al. (2010) On the condition number distribution of complex wishart matrices. *IEEE Trans. Commun.*, **58**(6): 1705-1717.
[72] Verdu, S. (1998) *Multiuser Detection* (Cambridge University Press), 1st ed.
[73] Jose, J. et al. (2009) Pilot contamination problem in multi-cell TDD systems. In *Proceedings of the IEEE ISIT*, 2184-2188.
[74] Farhang, A. et al. (2014) Pilot decontamination in CMT-based massive MIMO networks. In *Proceedings of the ISWCS*, 589-593.
[75] Farhang-Boroujeny, B. (2003) Multicarrier modulation with blind detection capability using cosine modulated filter banks. *IEEE Trans. Commun.*, **51**(12): 2057-2070.
[76] Godard, D. (1980) Self-recovering equalization and carrier tracking in two-dimensional data communication systems. *IEEE Trans. Commun.*, **28**(11): 1867-1875.
[77] Farhang-Boroujeny, B. (2013) *Adaptive Filters: Theory and Applications* (John Wiley & Sons, Inc.), 2nd ed.
[78] Madhow, U. and Honig, M. (1994) MMSE interference suppression for direct sequence spread-spectrum CDMA. *IEEE Trans. Commun.*, **42**(12): 3178-3188.